Available online at www.sciencedirect.com
SCIENCE DIRECT®
Cement and Concrete Research 36 (2006) 245 – 258
Cement and Concrete Research

Assessment of diffusive and mechanical properties of hardened cement pastes using a multi-coated sphere assemblage model

B. Bary *, S. Béjaoui

CEA Saclay, DEN/DPC/SCCME/LECBA, 91191 Gif/Yvette, France

Received 25 April 2004; accepted 17 July 2005

Abstract

This paper addresses the problem of the estimation of the diffusive and mechanical properties of hardened cement pastes by means of a simplified multi-coated sphere assemblage model. This model relies on a microstructure description involving the main hydrated products (portlandite, C–S–H, and aluminous compounds) and accounts for the physical properties of each phase as well as their volume fraction and to a certain extent their size and relative disposition. The basic idea is that any initial cement grain hydrates partly to form an external (outer) layer of C–S–H and partly an internal (inner) layer of C–S–H, both having different properties. The multi-coated sphere model, due to Hashin for its 2-phase version, is then used and applied to calculate the diffusion coefficient and Biot coefficient of such an assemblage. The evolutions of the diffusive properties when the initial material is subjected to lixiviation and calcite formation are estimated on the basis of simplified description of these degradation mechanisms; the issue of expansion due to internal pressure generated by crystal growing (crystallization pressure) in the context of sulfate attack is also analyzed.

Keywords: Diffusion; Mechanical properties; Sulfate attack; Numerical simulation; Modeling

1. Introduction

The long-term behavior of cementitious materials is a topic of great concern in many applications of civil engineering. In particular, such materials are already widely used for radioactive waste conditioning and containers and could become an attractive option for the construction of disposal engineering barriers, surface structures and underground structures for interim and long-term storage, respectively [1,2]. In this context the French Atomic Energy Commission (CEA) has developed research programs aiming at analyzing and characterizing the long-term behavior of cement-based materials. Several degradation scenarios have been identified and analyzed in condition of water immersion or flow (as a consequence of ground water), for which the diffusive and mechanical properties are of particular importance. In this study we focus our attention on these two properties and their evolutions induced by the following chemical attacks (or the consequences of these chemical attacks), in the case of saturated cement pastes: leaching (decalcification), carbonation and swelling due to sulfate attack.

Whereas many studies have been devoted to the analysis and the characterization of physical properties of concrete viewed as a heterogeneous material made up of aggregates surrounded by cement paste matrix with or without interfacial transition zone (see e.g. [3–5]), few address this problem at the level of the cement paste. However, a better understanding of the global performance of complex materials such as Portland cement-based ones requires investigations and knowledge at a microstructural level [6]. In particular, if we examine the case of two cement pastes made with CEM I and CEM V cement, respectively, both having the same water to cement ratio (w/c), experimental results show a higher global porosity for CEM V material, whereas the diffusive coefficient is one order greater for CEM I paste (see e.g. Ref. [7]). This observation indicates that the total porosity, which is a macroscopic quantity, cannot be considered as a suitable parameter for assessing the diffusion parameter when dealing with different materials.

The microstructure description of the hydrated cement paste adopted in this study is based on a very simple microstructure

* Corresponding author. Tel.: +33 1 69 8 23 83; fax: +33 1 69 8 84 41.
E-mail address: bary@azurite.cea.fr (B. Bary).

0008-8846/$ - see front matter © 2005 Elsevier Ltd. All rights reserved.
doi:10.1016/j.cemconres.2005.07.007

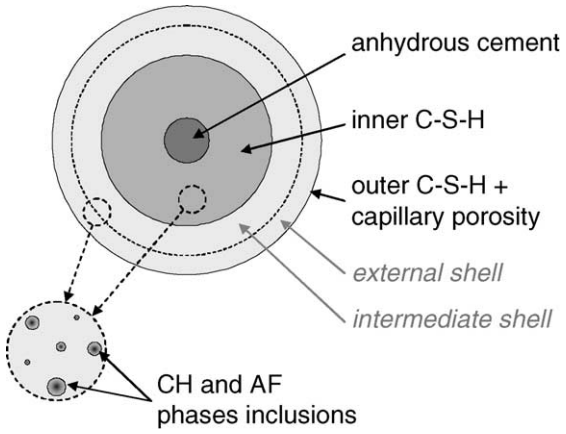

Fig. 1. Elementary description of the composite sphere forming the hydrated cement paste; spherical inclusions of portlandite and aluminous phases are distributed through both inner and outer C–S–H.

description of the cement paste involving only the four following components: internal and external calcium silicate hydrate phase (C–S–H), calcium hydroxide (CH), aluminous phases (AF) and anhydrous compounds. It relies on the basic idea that any initial cement grain hydrates in a first stage to form an external (outer) layer of C–S–H. When the available space becomes limited for the hydrated products to develop, together with the fact that the water reaches the anhydrous cement with more and more difficulty (due to the C–S–H layer growing), then a more compact internal (inner) C–S–H layer forms [6,8]. Both CH and aluminous phases are supposed to be dispersed as inclusions of different sizes in the two C–S–H layers. We investigate and propose to model the changes of diffusive properties under steady-state and saturated conditions when the material is subjected to leaching (decalcification of the hydrated products) and carbonation. Further, we propose to apply our approach to give a comprehensive and theoretical description of the material expansion due to an internal crystallization pressure generated by sulfate attack.

2. Bases of the model

The approach adopted in this study for describing the microstructure of the Portland cement paste relies basically on the assumption that the cement grains are initially spherical (typically in the range 0.1 to 100 μm and more [9,10]) and that they hydrate in two main components (inner and outer C–S–H) to form an assemblage of doubly coated spheres, in which are inserted other minor hydrated products (CH and AF phases) as spherical inclusions, supposed to be perfectly bonded to the C–S–H matrix. The core corresponds to the anhydrous part of the cement grains remaining (or not) after complete hydration and is surrounded first by the inner C–S–H layer and second by the outer one, both forming concentric shells (Fig. 1).

The porosity is assumed to be of two types: the capillary porosity (with a size domain starting from about 0.2–0.3 μm) constituting a material phase and the nanoporosity (sizes inferior to 0.2–0.3 μm) supposed to be intimately mixed with C–S–H to form the C–S–H matrix phase. The outer layer is divided into an external and intermediate shell, both having different capillary porosity volume fraction but identical C–S–H matrix properties. The CH and AF phases are homogeneously, but with different total volume fractions, distributed within each of the two C–S–H phases as spherical inclusions of various radii, the highest size of which is supposed to be small compared to the dimensions of shells; this latter hypothesis is supported by experimental evidence (see e.g. Ref. [6–8]). The capillary porosity is also assumed to be embedded in the outer layer and will receive a special treatment in particular when addressing the diffusion problem. The composite spheres possess exactly the same volume fraction for each of the elementary phases and occupy the entire volume of the material, implying a distribution in their sizes ranging to the infinitesimally small (a two-dimensional representation of such a construction is given in Fig. 2). This assumption is introduced for the sake of simplicity and because it leads to assemblages having certain exact effective properties results. For real materials, the smallest of the composite spheres do not probably exist and we assume these ones do not affect significantly the global behavior. All the initial phases are supposed to be isotropic and homogeneous and so is the macroscopic behavior of the material. The resulting well-known composite sphere model has been introduced in a two-phase version by Hashin [11] and then has been extended to multi-coated spheres by numerous researchers for evaluating physical properties such as conductivity (or diffusion) and mechanical parameters for multiphase materials (see e.g. Refs. [12–16]). It is worth noting here that by diffusion we mean mass transfer generated by concentration gradients of aqueous species; the porous medium is considered totally saturated and we neglect electrodiffusive phenomena due to electric charge of the ionic particles.

The evaluation of the effective physical properties for the material needs the knowledge of properties of each elementary phase. It means that a multiphase effective-medium approximation is required for assessing the properties of both inner and outer phases, where CH and AF spherical inclusions are

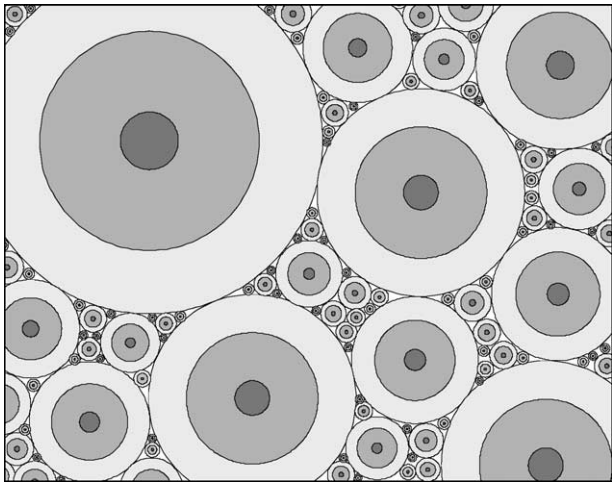

Fig. 2. Two-dimensional representation of the composite sphere assemblage describing the hydrated cement paste.

embedded. In the ensuing developments, the Maxwell approximation will be used due to its simplicity, although the total volume fraction of the inclusions may be relatively high (up to 0.4). However, the characteristics of percolation threshold of the self-consistent (SC) scheme will be utilized for diffusion applications, as will be explained in the next section.

3. Evaluation of the diffusion coefficient for the intact and degraded material

3.1. Estimation of the effective diffusion coefficient for the intact material

We refer to and extend the 3-dimensional microstructural representation of the hydrated cement paste detailed in the previous section for estimating the diffusion coefficient, where this material is viewed at first as a multi-coated sphere assemblage. The effective diffusivity $\bar{D}$ of such a 3-phase material is well known and takes the form (see e.g. [13,17]):

$$\bar{D}= D_3 + (1-\phi_3)\left\{\left[D_2 - D_3 + \xi\left[(D_1-D_2)^{-1} + (1-\xi)(3D_2)^{-1}\right]^{-1}\right]^{-1} + \frac{\phi_3}{3D_3}\right\}^{-1}, \quad (1)$$

where $\xi=\phi_1/(\phi_1+\phi_2)$, D_i and ϕ_i are the diffusion coefficient and volume fraction of phase i and the subscripts 1, 2, 3 denote the core, first and second coating (inner and outer C–S–H), respectively. It is shown that this result is obtained by determining the local fields on a single composite sphere. The basis of the method consists in considering a homogeneous body with unknown diffusion coefficient $\bar{D}$ subjected to a uniform field $\boldsymbol{E}$ throughout it. Then a sphere of radius $\boldsymbol{r}$ within the body is replaced by a composite sphere of the same radius. The value of $\bar{D}$ for which the field outside the sphere remains unchanged is the solution of the problem; indeed, repeating this replacement process until the whole body is replaced by composite spheres leads to a 3-phase coated-sphere dispersion with diffusivity $\bar{D}$.

To be more general, the previous approach can be straightforwardly extended to $(n+1)$-coated sphere assemblages. By adopting the notation of the Fig. 3 for the $(n+1)$ different elementary phases of an n-coated sphere, the effective diffusion coefficient $\bar{D}_{n+1}$ of the composite sphere construction is determined by the following expression:

$$\bar{D}_{n+1} = D_{n+1} + (1-\xi_{n+1})\left[\left(\bar{D}_n - D_{n+1}\right)^{-1} + \frac{\xi_{n+1}}{3D_{n+1}}\right]^{-1}, \quad \text{with} \quad \xi_{k+1} = \phi_{k+1}\left(\sum_{j=1}^{k+1}\phi_j\right)^{-1}, \quad (2)$$

where $\bar{D}_n$ denotes the effective diffusion coefficient associated with the $(n-1)$-coated sphere model; for completeness, it is stated that $\bar{D}_1=D_1$. The parameter ξ_{k+1} is such that $\xi_{n+1}=\phi_{n+1}$ for the $(n+1)$-phase material and corresponds to the volume fraction of the phase $(k+1)$ with respect to the volume fraction sum of phases 1 to $(k+1)$. This form appears to be more compact than other expressions generally found in the literature. By setting $(n=1)$ in Eq. (2) and given that $\xi_2=\phi_2$ in this case, the well-known formula providing the effective diffusion coefficient $\bar{D}_2$ for a two-phase sphere assemblage model is obtained:

$$\bar{D}_2 = D_2 + (1-\phi_2)\left[(D_1-D_2)^{-1} + \frac{\phi_2}{3D_2}\right]^{-1}. \quad (3)$$

As noted previously, Eq. (2) can be simply viewed as a generalization of Eq. (3); indeed, the reasoning for obtaining $\bar{D}_{n+1}$ relies on the fact that the $(n-1)$-coated sphere material corresponding to the elementary phases 1 to n and characterized by its effective diffusion coefficient $\bar{D}_n$ can be interpreted as a single phase forming the core of a two-phase sphere model. This observation permits to apply again Eq. (3) to establish a relation between $\bar{D}_{n+1}$ and $\bar{D}_n$, with particular attention paid to the determination of the equivalent volume fraction ξ_{n+1} of the $(n+1)$th coating (see e.g. Ref. [17]).

Given the expression of the effective diffusion coefficient for the $(n+1)$-layered sphere assemblage (see Eq. (2)), the problem is now to estimate the diffusivity for the elementary shell. This problem can be divided in two parts: first, we need to assess the diffusive parameter of the C–S–H matrix (which can be a priori provided directly by experiments) and, second, the effects of the spherical inclusions of CH, AF and capillary porosity (for outer C–S–H shell) embedded in the C–S–H matrix have to be evaluated. We assume that the scale of these two sub-problems is different; indeed, the typical size of the inclusions ranges from less than 1 ìm up to several tens of micrometer for massive crystals, whereas the characteristic length scale of C–S–H is 1 to 100 nm [9]. Because of its much higher diffusivity than the other components (AF and CH are supposed to be perfectly insulating), the characteristics of connectedness and thus of percolation of the capillary porosity are of great importance with respect to the diffusion. It is proposed to treat this phase specifically as follows. The existence of a volume fraction

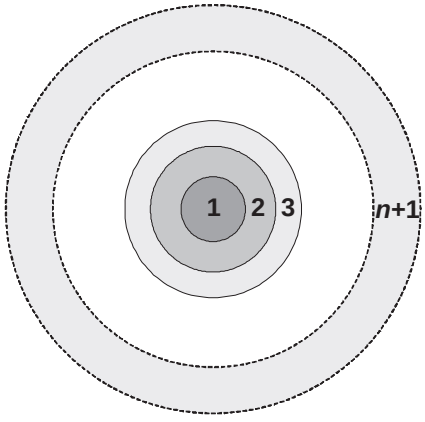

Fig. 3. Two-dimensional representation of a $(n+1)$-layered composite sphere.

threshold under which the capillary porosity is not connected is assumed, this latter phase being introduced as spherical inclusions in the outer C–S–H shell. The fraction of capillary porosity above this threshold is considered to be connected and forms, together with C–S–H matrix and both CH and AF inclusions, an additional shell with higher proportion of capillary porosity; this layer constitutes the external shell of the outer C–S–H, whereas the intermediate shell is the remaining part of the outer C–S–H, as defined in Fig. 1. The outer C–S–H is then divided into two separate layers; for the external one (which percolates), it is proposed to use the SC scheme to estimate its diffusive properties, whereas for the intermediate shell, where no particular percolation properties are to be introduced, the Maxwell's approximation is applied. It is well known that the SC scheme does not predict the percolation at the correct volume fractions; its use simply permits to introduce artificially a percolation threshold in the modeling, which has no physical signification and therefore has to be adjusted on experimental data. It is worth noting that this notion of capillary porosity threshold has been utilized in other contributions (see e.g. Ref. [18]). The Maxwell approximation, when generalized to suspensions with two different types of spherical inclusions, leads to the following expression for the effective diffusion coefficient D_k of the (k)th layer of the composite sphere (see e.g. Ref. [16]):

$$\frac{D_k - D^{(k)}}{D_k + 2D^{(k)}} = \sum_{i=1}^{2} \phi_k^{(i)} \left[\frac{D^{(i)} - D^{(k)}}{D^{(i)} + 2D^{(k)}} \right] \tag{4}$$

with $D^{(k)}$ the diffusion coefficient of the C–S–H matrix phase and $D^{(i)}$ the diffusion coefficient of the i^{th} inclusion of volume fraction $\phi_k^{(i)}$ with respect to the layer k. This expression is also given by the Mori-Tanaka method [16]. If we consider that both CH and AF inclusions are perfectly insulating relative to the C–S–H phase, i.e. $D^{(i)}/D^{(\text{inn})}=0$, the previous expression for the inner C–S–H reduces to:

$$D_{\text{inn}} = 2D^{(\text{inn})} \left[1 - \sum_{i=1}^{2} \phi_{\text{inn}}^{(i)} \right] \left[2 + \sum_{i=1}^{2} \phi_{\text{inn}}^{(i)} \right]^{-1} \tag{5}$$

due to the absence of capillary porosity. For the intermediate shell of the outer C–S–H, a fraction of the capillary porosity $\phi_{\text{int}}^{(\text{cp})}$ has to be introduced as inclusions of much greater diffusivity than the matrix; in the limiting case $D^{(\text{out})}/D^{(\text{cp})}=0$, one gets:

$$D_{\text{int}} = D^{(\text{out})} \left[1 + 2\phi_{\text{int}}^{(\text{cp})} - \sum_{i=1}^{2} \phi_{\text{int}}^{(i)} \right] \left[1 - \phi_{\text{int}}^{(\text{cp})} + \frac{1}{2} \sum_{i=1}^{2} \phi_{\text{int}}^{(i)} \right]^{-1}. \tag{6}$$

The application of the SC scheme to the estimation of the effective diffusion coefficient D_{ext} of the outer C–S–H external shell (composed of 3 phases) leads to the classical following relation, where the previous notations still hold:

$$D_{\text{ext}} = \frac{1}{4} \left[\alpha + \sqrt{\alpha^2 + 8D^{(\text{out})} D^{(\text{cp})} \left(1 - \frac{3}{2} \left(\sum_{i=1}^{2} \phi_{\text{ext}}^{(i)} \right) \right)} \right], \text{ with}$$
$$\alpha = D^{(\text{out})} \left(2 - 3 \left(\phi_{\text{ext}}^{(\text{cp})} + \sum_{i=1}^{2} \phi_{\text{ext}}^{(i)} \right) \right) + D^{(\text{cp})} \left(3\phi_{\text{ext}}^{(\text{cp})} - 1 \right). \tag{7}$$

The superscripts out, cp and i refer to the outer C–S–H matrix, capillary porosity and both AF and CH inclusions, respectively; these latter inclusions are considered to be perfectly insulating. It should be noted that for the limiting case $D^{(\text{out})}/D^{(\text{cp})}=0$ this relation becomes:

$$\frac{D_{\text{ext}}}{D^{(\text{out})}} = \frac{1 - \frac{3}{2} \left(\sum_{i=1}^{2} \phi_{\text{ext}}^{(i)} \right)}{1 - 3\phi_{\text{ext}}^{(\text{cp})}}. \tag{8}$$

3.1.1. Application

To illustrate the method presented above, we propose to apply it to the estimation of the effective diffusion coefficient for CEM I hydrated cement pastes with various w/c. The main characteristics and numerical data for the materials are drawn from Ref. [7] and are listed in Table 1. The volume fractions of the different compounds have been evaluated by making use of Jennings model [19]; see Ref. [7] for the details and the hypotheses of the calculations.

For Eqs. (5), (6) and (7) to be applicable, the determination of the diffusion coefficients and the percolation threshold are required. Setting $D^{(\text{cp})}=2.0\ 10^{-9}$ m^2/s [7] and assuming that the percolation threshold is equal to 8%, we propose to identify the diffusive properties of both inner and outer C–S–H by confronting numerical calculations performed with Eqs. (5), (6) and (7) and experimental measurements of tritiated water

Table 1
Composition in volume fraction of the hydrated cement pastes [7]

w/c	Capillary porosity	AF	CH	Anhydrous	Inner C–S–H	Outer C–S–H	Inclusion outer/inner (%)
0.30	7.1	14.6	15.2	13.7	37.4	12.0	12.0/37.4
0.35	9.7	14.7	15.6	9.4	33.9	16.8	16.8/33.9
0.40	12.7	14.5	15.5	6.4	28.3	22.6	22.6/28.3
0.45	15.9	14.2	15.1	4.3	21.6	28.8	28.8/21.6
0.50	19.2	14.0	14.4	3.0	14.6	34.8	34.8/14.6
0.60	25.0	12.6	13.1	1.4	1.0	47.0	47.0/1.0

diffusion coefficient taken from Ref. [7]. The numerical results obtained with the set of values $D^{(out)}=3.4\ 10^{-12}$ m^2/s and $D^{(in)}=8.3\ 10^{-13}$ m^2/s are depicted on Fig. 4 and compared to experiments. We note that these results agree relatively well; the maximal variation, less than 15%, is observed for a w/c ratio equal to 0.30. It should be emphasized that these results are largely dependent on the distribution and volume fraction of the initial constituents as given in Table 1. Because these quantities are mainly obtained by simulations [7], they need to be validated and consolidated by further experimental observations and characterizations on real microstructures, which constitute an essential aspect to investigate in the future. Moreover, some of the assumptions made are material dependent in the sense that they require a priori to be adjusted for other types of cement pastes; in particular, the percolation threshold for the capillary porosity as introduced in the external shell of the outer C–S–H would probably be different for CEM V cement pastes for example.

3.2. Estimation of the effective diffusion coefficient for the material subjected to leaching

The above procedure is now applied for estimating the effective diffusion coefficient in the case of a saturated hydrated CEM I cement paste subjected to a decalcification process by pure water. According to the description of the leaching phenomenon generally accepted in the literature for materials prepared with CEM I cement (see e.g. Refs. [8,9,20,21]), the main aspects to consider are, first, the CH phase dissolves completely when the calcium concentration in the pore solution (C_a) decreases and, second, the C–S–H phase, which is characterized by a calcium over silicon (C/S) ratio for the intact material of around 1.65, progressively decalcifies when the decrease of C_a continues; this decalcification is accompanied by a progressive drop of C/S ratio from 1.65 to approximately 0.8. As for the aluminous phases AF, their decalcification is also supposed to occur progressively but initiates when C–S–H degradation process is engaged and ends roughly when C–S–H is totally decalcified. A key point is that, with a good accuracy, this degradation process can be described by using only one variable: the calcium concentration in the pore solution C_a. It will be then assumed that this variable governs the dissolution phenomena and that these latter occur at chemical equilibrium. Moreover, we suppose that the total concentration of calcium in solid phases (which characterizes the degradation level of each elementary phase composing the material) can be uniquely related to C_a by multilinear functions (see for more details Refs. [22,23]). To illustrate these hypotheses, consider the cement paste with $w/c=0.4$ as defined in Table 1. A simplified calculation allows estimating the molar proportion of each of the elementary compounds per unit volume of material by making use of the well-known Bogue formula. With this example we get C–S–H=5292 mol/m^3, CH=5689 mol/m^3, and AF=330 mol/m^3 (the AF phase is supposed to be composed only of mono-sulfoaluminate for the sake of simplicity).

The degradation process is then assumed to be schematically described by Fig. 5, showing the progressive decrease of the calcium concentration in the solid phase S_{ca} as a function of C_a. This result has been obtained by using and adapting the numerical results performed with the code CHESS developed at Ecole des Mines (see e.g. Ref. [24]), which solves chemical equilibrium problems. The following hypotheses are supposed to apply: no alkalis are present in pore solution and the C–S–H decalcification is described (discretized) by 3 distinct phases with C/S ratios of 1.65, 1.25 and 0.90, respectively. In Fig. 5 is also depicted a linear simplification of the CHESS results, which eliminate the strong variations of S_{ca} occurring when a phase disappears (is totally decalcified). In this context, C_a can then be viewed as an indicator of the degradation state when regarding the decalcification process.

It is proposed simply to adapt Eq. (3) for dealing with the case of the C–S–H matrix phases. We then assume that both inner and outer C–S–H matrix are composed only of a

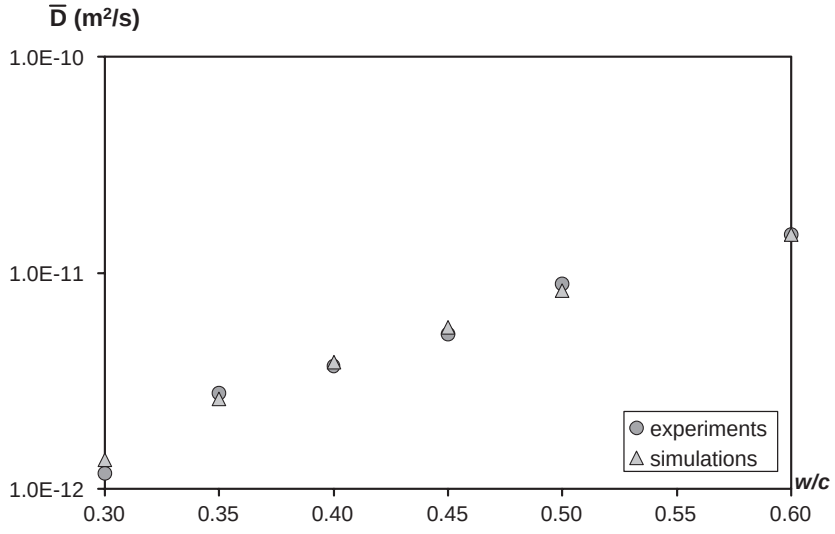

Fig. 4. Numerical and experimental (tritiated water, [7]) effective diffusion coefficient for CEM I hydrated cement paste with various w/c ratios.

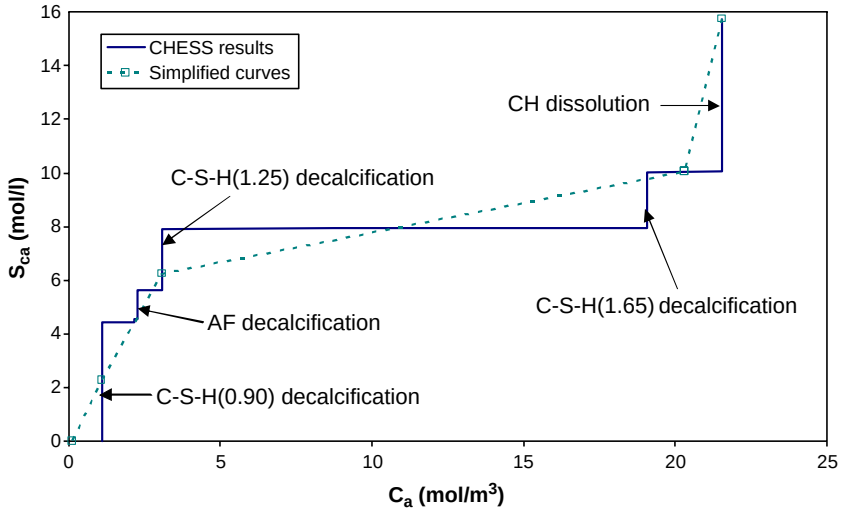

Fig. 5. Degradation process of the main hydrated phases in terms of calcium concentration in solid phase S_{ca} as a function of calcium concentration in solution C_a (line=results obtained with the chemical equilibrium code CHESS; dotted line=simplified curve).

perfectly insulating solid phase and a phase corresponding to the nanoporosity and form an assemblage of coated spheres with sizes ranging to the infinitesimally small. Further, we suppose that the total porosity in each C–S–H matrix is divided into a percolating part and an occluded one, this latter being embedded in the solid phase; consequently the core of each coated sphere is the sum of the solid phase and the non-percolating nanoporosity. Using Eq. (3) in which the diffusion coefficient of the composite spheres core is 0, the resulting diffusion coefficient $D^{(k)}$ of the C–S–H matrix is given by:

$$D^{(k)} = D^{(\mathrm{p})} \frac{2\phi_k^{(\mathrm{p})}}{3 - \phi_k^{(\mathrm{p})}} \tag{9}$$

where $D^{(\mathrm{p})}$ and $\phi_k^{(\mathrm{p})}$ denote the diffusion coefficient and the volume fraction of the saturated percolating porosity, respectively. In the following application, the values retained are $D^{(\mathrm{p})}=2.5\ 10^{-10}$ m^2/s, $\phi_{\mathrm{in}}^{(\mathrm{p})}=0.005$ and $\phi_{\mathrm{out}}^{(\mathrm{p})}=0.02$, which yield the values taken for $D^{(\mathrm{out})}$ and $D^{(\mathrm{in})}$ in the previous section. An additional percolating porosity of 0.05 is assumed to arise during the decalcification process of the C–S–H.

To apply the method to the case of leaching, some further assumptions regarding the decalcification mechanism of the hydrated phases have to be made. Firstly, we suppose that CH inclusions embedded in each layer dissolve totally and are replaced by capillary porosity. Secondly, we assume that, at the end of the leaching process, only a fraction of the initial volume of AF and C–S–H phases are replaced by capillary porosity (in the numerical applications, the following values are used for AF and C–S–H: 50% and 5%, respectively, the latter value being taken from [9]). Lastly, the degradation is supposed to be, in term of dehydrated volume (that is, volume of solid phase replaced by porosity), linearly related to the calcium concentration in pore solution C_a according to Fig. 5: CH dissolves between $C_a=21.54$ and $C_a=20.31$ mol/m^3, C–S–H between

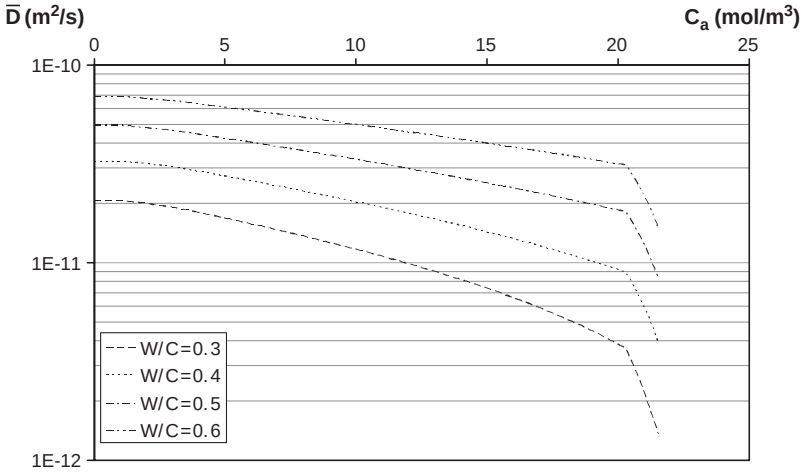

Fig. 6. Evolutions of the effective diffusion coefficient for 4 different cement pastes (of which composition is defined in Table 1), as a function of calcium concentration in pore solution.

C_a=20.31 and C_a=1.09 mol/m^3, and AF between C_a=20.31 and C_a=8.081 mol/m^3.

The effective diffusion coefficient versus calcium concentration for cement pastes with different w/c ratios, with compositions listed on Table 1, are shown on Fig. 6. The effective diffusion coefficient is multiplied by a factor of about 2 to 3 when CH is totally dissolved. From the beginning to the end of the degradation process, the increase of this parameter is up to one order of magnitude for the lowest w/c ratio and a factor of 4 for the greater one. It is noteworthy that both initial and final values obtained for w/c=0.4 are close to the ones reported in Ref. [7] for a similar material. The method yields the evolution of the total porosity during leaching. Numerical results obtained for cement pastes of different w/c ratios are gathered on Fig. 7. There is a strong increase in porosity when the CH inclusions dissolve. Both initial and final values of the porosity are consistent with experimental results obtained in Ref. [25] by mercury intrusion porosimetry, for a comparable material with w/c ratio equal to 0.45: $\phi_{ini} \approx 0.20$ and $\phi_{fin} \approx 0.52$.

3.3. Estimation of the effective diffusion coefficient for a carbonated material

This section is devoted to the evaluation of the effective diffusion coefficient when the cement paste is subjected to carbonation in saturated conditions, that is, when calcium ions react with carbonate ions present in pore solution and precipitate into calcite. It is proposed to express the carbonation influence on the diffusive properties, for different volumes of precipitated calcite, as a function of calcium concentration in pore solution, this latter variable being again interpreted as a descriptor of the decalcification state. This choice is equivalent to considering that a fraction of the volume of decalcified solid phases is replaced by calcite, corresponding to a material submitted first to combined leaching and carbonation, and then after achievement of a certain carbonation degree, subjected only to leaching. This carbonation degree is supposed to be characterized by the volume fraction of precipitated calcite. When addressing the phenomenon from the modeling point of view, the drop of diffusion coefficient due to calcite precipitation is usually explained by a reduction of the global porosity, with in general no consideration paid to the material degradation (decalcification) level. In this study this latter aspect is taken into account. It is supposed that the calcite precipitates first in the capillary porosity sites, whatever the decalcification state. Then, if the hydrated products provide no space because they are not decalcified, the C–S–H phases are assumed to be calcified (that is, filled with calcite, which leads to reduction of nanoporosity, cf Eq. (9)) up to a C–S–H matrix diffusion threshold below which the formation is no longer possible; this threshold has been fixed for both C–S–H types to 1.6 10^{-13} m^2/s, in order to obtain an effective diffusion coefficient when the material is totally carbonated of 9.0 10^{-14} m^2/s, corresponding to an experimental value drawn from Ref. [7]. Now if decalcification is initiated, calcite formation first takes place in the sites left by CH inclusions, then by C–S–H and AF decalcification.

These hypotheses and conditions lead to the results presented on Fig. 8. The case of the cement paste with w/c ratio of 0.35 and formulation detailed in Table 1 has been simulated for several values of maximum calcite volume fraction, ranging from 0 to 0.32. The lowest value of diffusion coefficient is obtained obviously when the material exhibits the lowest global porosity level, whatever the decalcification degree; it appears first for a calcite volume fraction of 0.198 which corresponds to the sum of the capillary porosity and the C–S–H matrix filling. The capillary porosity has a significant effect on the diffusion coefficient because its filling has a strong impact on the diffusion and percolation properties. The importance of C–S–H and AF decalcification can be deduced from examination of the curves for calcite volume fractions of 0.32 and 0.28, which exhibit a significant increase for low C_a values.

4. Estimation of the global mechanical effects due to internal pressures generated by sulfate attack

This section is devoted to the evaluation of the mechanical response of the material when it is subjected to internal

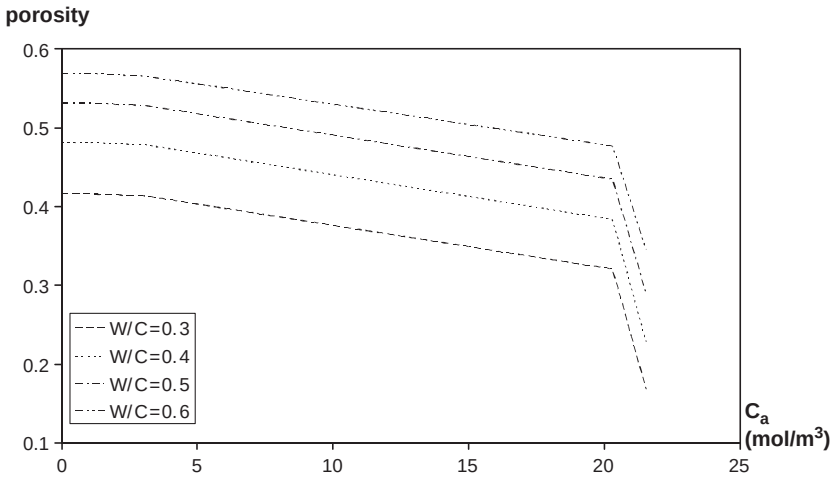

Fig. 7. Evolutions of the porosity for 4 different cement pastes (of which composition is defined in Table 1), as a function of calcium concentration in pore solution.

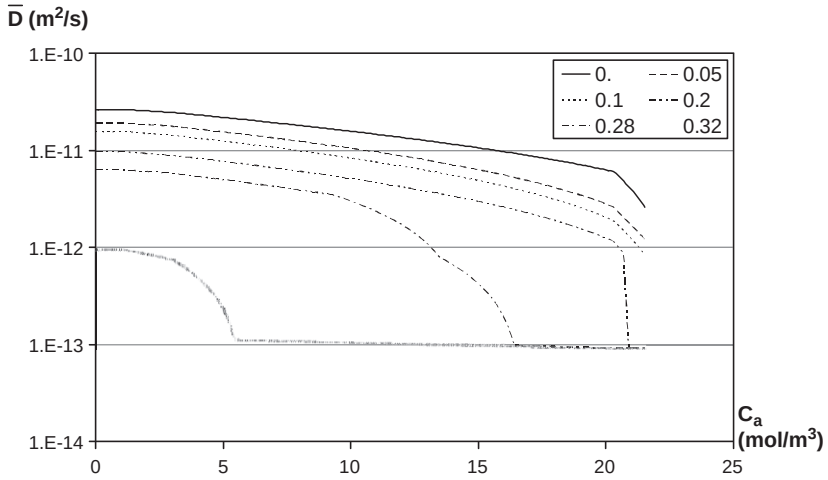

Fig. 8. Evolutions of the effective diffusion coefficient for a cement paste with w/c ratio of 0.35, subjected to carbonation with different levels (the maximum volume fraction of calcite is indicated in the legend), as a function of calcium concentration in pore solution.

pressures generated by chemical reactions consecutive to sulfate attacks. The topic of sulfate attacks has been intensively studied by many researchers, from chemical and coupled chemo-transfer points of view (see e.g. Refs. [8,26–29]; however, up to now relatively few approaches exist regarding the treatment of the global chemical–mechanical-transfer problem [30]. In this study it is proposed to deal with the chemo-mechanical part of this subject by means of micro-mechanical considerations and on the basis of the material microstructural description developed in Section 2. It will be assumed that the major phenomena leading to pressure generation and swelling are similar in the cases of delayed ettringite formation (DEF) and external sulfate attack.

4.1. Expansion mechanism due to sulfate attack

The expansion process is supposed to result from crystallization pressures due to the interaction between the solid product of chemical reactions (ettringite) and the surrounding cement paste [31,32]. This approach then suggests that chemical energy is converted into mechanical work whenever the solid product is confined, the driving forces being the activities of the reactants (supersaturations) in the pore solution. Precisely, it is assumed that the expansion mechanism can be schematically explained by the pressures generated by crystal growth due to monosulfate inclusions reacting to form ettringite in the presence of calcium and sulfate ions in pore solution. The pressures are significantly higher when the initial crystals are intimately mixed with the surrounding C–S–H matrix and the reactions occur in confined spaces at high supersaturation [26,33]. Although this mechanism can be extended to the case of gypsum, which also precipitates in the presence of sufficient calcium and sulfate concentrations in pore solution and therefore may create crystallization pressures [31], it will be neglected in the ensuing discussion. It has been emphasized that the pressure intensity is strongly related to the confinement of growing crystals; this leads to the conclusion that the maximal pressure values are obtained in the zones with dense C–S–H matrix and high volume fractions of (initial) monosulfate. According to Ref. [26], these zones are located in the outer C–S–H shell immediately surrounding the inner one; indeed, with increasing distance away from the core of cement grain, the porous structure becomes more open, lessening the conditions for maximizing pressures. It is supposed that there is initially no sufficient quantity of monosulfate in the inner C–S–H shell to produce substantial pressures.

The crystallization pressure can be expressed by means of the thermodynamic principle of crystallization pressure in the following way (see e.g. Refs. [31,33]). We suppose that the chemical reaction under consideration may take the form $\gamma_i R_i \leftrightarrow S$, where γ_i is the stoichiometric coefficient of the i^{th} reactant R_i and S is the solid product of the reaction. The equilibrium state of this reaction imposes that $\mathrm{d}\mu_s = \gamma_i \mathrm{d}\mu_i$, with μ_s the chemical potential of the solid product and μ_i the one for the reactant R_i. Assuming S is subjected only to the hydrostatic pressure p_h, we can express $\mathrm{d}\mu_s$ and $\mathrm{d}\mu_i$ as:

$$\begin{aligned} \mathrm{d}\mu_s &= -s_s \mathrm{d}T + v_s \mathrm{d}p_h, \\ \mathrm{d}\mu_i &= \mathrm{d}\bar{\mu}_i + \mathrm{d}(RT\ln(a_i)) = \mathrm{d}\bar{\mu}_i + R\ln(a_i)\mathrm{d}T + RT\mathrm{d}\ln(a_i) \end{aligned} \tag{10}$$

where s_s and v_s are the molar entropy and molar volume of solid product, $\bar{\mu}_i$ is the chemical potential of R_i at standard state, function of the temperature T and the pressure of liquid phase p_l, and a_i is the activity of R_i in the solution. Under the conditions that both T and p_l are constant, $\mathrm{d}\bar{\mu}_i(T,p_l)$ is zero and the last two relations can be simplified in:

$$dp_h = \frac{RT}{v_s}\gamma_i \mathrm{d}\ln(a_i). \tag{11}$$

Integrating this expression and introducing a reference state (superscript 0) where there is no interaction between the solid product and the cement paste yield:

$$p_c = p_h - p_h^0 = \frac{RT}{v_s}\ln\left(\frac{a_i}{a_i^0}\right)^{\gamma_i} = \frac{RT}{v_s}\ln\left(\frac{K_{sp}}{K_{sp}^0}\right) \tag{12}$$

where $K_{sp} = a_i^{\gamma i}$ and $K_{sp}^0 = a_i^{0\gamma i}$ refer to the solubility product of S under pressure p_h and p_h^0, respectively; the pressure p_h^0

without interaction can be chosen to the atmospheric pressure. Denoting p_c as the interaction pressure resulting from reactant activity increases in pore solution and crystal growth prevention, it appears that p_c is the essential cause of sulfate expansion and exerts on both the solid product and the C–S–H matrix. As emphasized in Refs. [31,26], the two necessary conditions for crystallization pressure to produce expansion are the confinement of crystal growth and the fulfillment of the inequality $K_{sp} > K_{sp}^0$, that is, the supersaturation of reactants. In this study, the first condition is assumed to be realized, with different levels of confinement for the outer layer. Indeed, this level will be maximum in the intermediate C–S–H shell (in conjunction with the quantity of monosulfate), whereas in the external shell, which contains a priori an important volume fraction of capillary porosity (0.5 in the numerical simulations presented in the previous section), this level is lesser due to its more deformable structure. The second condition is also supposed to be fulfilled and, as appears clearly in Eq. (12), the driving forces imposing the magnitude of the crystallization pressure are defined by the activities a_i of the reactants.

4.2. Mechanical behavior of the cement paste subjected to sulfate attack

It is proposed in this section to evaluate the mechanical response of the material described in Sections 2 and 3 when it is submitted to sulfate attack characterized by a crystallization pressure p_c as expressed by Eq. (12). This pressure will be viewed in the ensuing discussion as an external loading parameter controlled by the following ionic species in pore solution: Ca^{2+}, SO_4^{2-} and Al^{3+}, which activity is supposed to be imposed. It is proposed to find an approach on the basis of the Biot formulation principle, where the macroscopic stress $\boldsymbol{\Sigma}$ acting on the material is decomposed into a part due to the macroscopic strain $\boldsymbol{E}$ and another one resulting from an internal pressure p^*, via the relation (see e.g. Refs. [34–36]):

$$\boldsymbol{\Sigma} = C^{\mathrm{h}} : \boldsymbol{E} - \boldsymbol{B}p^* \tag{13}$$

where C^{h} is the (homogenized) fourth-order stiffness tensor of the overall material and $\boldsymbol{B}$ is the second-order Biot tensor. The main objective of this section resides now in the estimation of these two macroscopic tensors, providing the knowledge of the mechanical properties of the elementary phases composing the material. As in the case of the diffusive properties, two stages have to be considered: one is the estimation of the overall parameters of the multi-coated sphere model as represented on Fig. 3, in which the different phases are constituted by the layers, regarded as homogeneous in this section, composing each sphere. The second stage consists in the evaluation of the mechanical parameters of these layers, given that they are formed with several types of inclusions embedded in the C–S–H matrix (see Fig. 1). In the following, our attention will be focused on the mechanical response of this construction undergoing an internal pressure. All phases will be assumed to have isotropic linear elastic behavior (except the saturated capillary porosity which will be considered, from a mechanical point of view, as void) and each shell of the composite sphere will be supposed to exhibit a homogeneous distribution of inclusions; consequently, without any other loading than this pressure, the response of the material is expected to be hydrostatic in terms of both macroscopic strain and stress fields.

5. Determination of the Biot coefficient for the multi-coated sphere model

This section addresses the issue of determining the Biot coefficient of the composite sphere model as described in Figs. 2 and 3. Each phase i will be considered as a homogeneous isotropic linear elastic porous medium saturated with fluid undergoing a uniform pressure p^*, with shear and bulk moduli μ_i and k_i, and Biot coefficient b_i, respectively; these parameters are supposed to be known. The local stress–strain relation for the phase i is defined by:

$$\boldsymbol{\Sigma}_i = 2\mu_i \boldsymbol{e}_i + k_i(\boldsymbol{E}_i : \boldsymbol{I})\boldsymbol{I} - b_i p^* \boldsymbol{I} \tag{14}$$

where $\boldsymbol{\Sigma}_i$, $\boldsymbol{E}_i$ and $\boldsymbol{e}_i$ are the local stress, strain and deviatoric part of the strain tensor, respectively. One first considers the case of a two-phase sphere model (that is, the case of Fig. 3 with $n=1$). Starting with the basic idea already employed in Section 3.1 concerning the diffusion coefficient estimation, such a composite sphere of radius $\boldsymbol{r}$ is inserted into an infinite homogeneous body obeying the macroscopic stress–strain relation (Eq. (13)). This body is subjected to prescribed uniform strain $\boldsymbol{E}$ and pore pressure p^*; the overall Biot coefficient $\bar{b}_2$ related to $\boldsymbol{B}$ by $\boldsymbol{B} = \bar{b}_2 \boldsymbol{I}$ will then be determined by making use of the condition that the sphere insertion does not provoke any perturbation in the body fields. Taking advantage of the elastic behavior and homogeneity of the phases (see for example Refs. [37,38]), the loading can be split into two distinct parts, such that the initial problem is equivalently replaced by the following two sub-problems: $(\boldsymbol{E}=0;\ p^*) \equiv P'$ and $(\boldsymbol{E}=p^*;\ 0) \equiv P''$. The total stress and strain are then simply obtained by summing their counterparts for both problems P' and P''. The latter one is well known and permits us to express explicitly the macroscopic bulk modulus $\bar{k}_2$ [11]. We focus our attention on problem P', which possesses spherical symmetry and consequently undergoes the classical displacement field $\boldsymbol{u}_i$ in phase i in the form:

$$\boldsymbol{u}_i = \left(c_i \boldsymbol{r} + \frac{d_i}{\boldsymbol{r}^2} \right) \boldsymbol{r} \tag{15}$$

where $\boldsymbol{r}$ is the radial vector emanating from the sphere and c_i and d_i are unknown constants. The determination of these four constants for $i=(1,2)$ results from the classical following continuity conditions for displacement and traction vector at the boundary surfaces core–shell (radius R_1) and shell–body (radius R_2) and the requirement of finite displacement in the core:

$$\begin{aligned} &\boldsymbol{u}_1(0) \quad \text{finite}, \qquad \boldsymbol{u}_1(R_1) = \boldsymbol{u}_2(R_1), \\ &\boldsymbol{\Sigma}_1(R_1)\boldsymbol{r} = \boldsymbol{\Sigma}_2(R_1)\boldsymbol{r}, \qquad \boldsymbol{u}_2(R_2) = 0. \end{aligned} \tag{16}$$

The continuity condition of the traction vector across the shell–body interface yields an expression connecting $\bar{b}_2$ and the mechanical parameters of the two-phase sphere:

$$\boldsymbol{\Sigma}_2(R_2)\boldsymbol{r} = \boldsymbol{\Sigma}(R_2)\boldsymbol{r} = -\bar{b}_2 p^* \boldsymbol{r}. \tag{17}$$

The solution of the problem (Eqs. (16) and (17)) leads to the exact relation:

$$\bar{b}_2 = b_2 + \frac{(3k_2+4\mu_2)(b_1-b_2)\phi_1}{4\mu_2+3k_1\phi_2+3k_2\phi_1}. \tag{18}$$

It can be noticed that this result corresponds to the well-known formula of Levin giving the overall thermal expansion coefficient $\bar{\alpha}_2$ for any two-phase material [39], providing the introduction of $\bar{k}_2$ in Eq. (18) and the replacement of $b_i p^*$ by $-3k_i\alpha_i\theta$ in local stress–strain relation (Eq. (14)) and $\bar{b}_2$ by $-3\bar{k}_2\bar{\alpha}_2$ in Eq. (13), for the case of thermoelastic behavior; α_i is the thermal expansion coefficient of the phase i and θ is the variation of temperature from initial conditions. The expression of the overall bulk modulus $\bar{k}$ is [11]:

$$\bar{k}_2 = k_2 + \frac{(3k_2+4\mu_2)(k_1-k_2)\phi_1}{4\mu_2+3k_1\phi_2+3k_2\phi_1}. \tag{19}$$

This relation has exactly the same structure as Eq. (18). Combining these two expressions yields:

$$\bar{b}_2 = \frac{b_1(\bar{k}_2-k_2)+b_2(k_1-\bar{k}_2)}{k_1-k_2}. \tag{20}$$

This result, when replacing the Biot coefficients by the thermal expansion ones, leads to the following relation due to Levin [39]:

$$\bar{\alpha}_2 = \frac{\alpha_1(1/\bar{k}_2-1/k_2)-\alpha_2(1/\bar{k}_2-1/k_1)}{1/k_1-1/k_2}. \tag{21}$$

It can be seen from Eq. (18) that the mechanical parameters of phase 1 (which defines the core of the composite sphere) enter into the expression for $\bar{b}_2$ only via its Biot coefficient and bulk modulus (the shear modulus does not appear). Since the latter is exactly known in the case of the $(n+1)$-layered sphere model and because the same is expected for the Biot coefficient (due to the correspondence between Eqs. (18) and (19)), it is suggested that the relation (Eq. (18)) can be straightforwardly extended to a multi-coated sphere assemblage model. Indeed, considering the $(n+1)$-phase construction of the Fig. 3, the relation (Eq. (18)) can be applied for determining its overall Biot coefficient $\bar{b}_{n+1}$, given that the elementary phases 1 to n are interpreted as a single phase with characteristics $\bar{k}_n$ and $\bar{b}_n$, which form the core of the two-phase sphere model of Eq. (18). One then has:

$$\bar{b}_{n+1} = b_{n+1} + \frac{(3k_{n+1}+4\mu_{n+1})(\bar{b}_n-b_{n+1})(1-\xi_{n+1})}{4\mu_{n+1}+3\bar{k}_n\xi_{n+1}+3k_{n+1}(1-\xi_{n+1})} \tag{22}$$

where ξ_{n+1} is defined in Eq. (2). For practical reasons, it can be useful to express $\bar{b}_3$ in a form involving only the elementary phase parameters:

$$\bar{b}_3 = b_3 + \frac{(3k_3+4\mu_3)(1-\phi_3)\{(b_2-b_3)(4\mu_2(1-\phi_3)+3\tilde{k}_{12})-\phi_1(b_2-b_1)(4\mu_2+3k_2)\}}{9k_1k_2\phi_3(1-\phi_3)+12\mu_2\tilde{k}_{12}\phi_3+(4\mu_3+3k_3(1-\phi_3))(4\mu_2(1-\phi_3)+3\tilde{k}_{12})} \tag{23}$$

with $\tilde{k}_{12}=k_2\phi_1+k_1\phi_2$ and $k_{12}=k_1\phi_1+k_2\phi_2$. Applying again the convenient replacement of b_i by $-3k_i\alpha_i$ and $\bar{b}_n$ by $-3\bar{k}_n\alpha_n$ for an extension of Eq. (22) to the case of thermoelasticity, the overall thermal expansion coefficient α_{n+1} of the $(n+1)$-phase composite sphere model is related to both elementary and overall properties by:

$$\bar{\alpha}_{n+1} = \frac{k_{n+1}}{\bar{k}_{n+1}}\alpha_{n+1} + \frac{(3k_{n+1}+4\mu_{n+1})(\bar{k}_n\bar{\alpha}_n-k_{n+1}\alpha_{n+1})(1-\xi_{n+1})}{k_{n+1}(4\mu_{n+1}+3\bar{k}_n\xi_{n+1}+3k_{n+1}(1-\xi_{n+1}))}. \tag{24}$$

This expression appears to be more compact than the one established recently in Ref. [38] but has the disadvantage of involving the overall bulk modulus $\bar{k}_{n+1}$.

5.1. Determination of the Biot coefficient for a layer of the sphere model

This subsection is concerned with the estimation of the parameters entering into the stress–strain relation (Eq. (14)) and in particular the Biot coefficient b_i. This coefficient will be evaluated by means of simple considerations and with the use of the superposition principle. As previously mentioned, the inclusions subjected to growing exert a pressure p^* theoretically defined by:

$$p^* = \langle p_c - p_E \rangle_+ = (p_c - p_E)\delta \tag{25}$$

with p_E as the pressure (hydrostatic part of the stress tensor) corresponding to the effect of the uniform loading strain $\boldsymbol{E}_i$ on the inclusions and $\delta = H(p_c - p_E)$ is the Heaviside step function applied to the argument $(p_c - p_E)$. Thus p^* expresses the fact that the effective pressure generated by the crystal growth results from the crystallisation pressure, p_c, corrected by the hydrostatic stress p_E due to the external mechanical loading applied on the crystals; p_c may then be related to the well-known concept of eigenstress (see e.g. Ref. [16]). If p_E is negative then p^* is lessened and if p_E is positive (corresponding to global tension), p^* increases. In other words, when the material undergoes (very) high compressive state of stresses, Eq. (25) suggests theoretically that there is no possibility for any crystal to form [33]. Because of the lack of information on this aspect, Eq. (25) is simplified as follows: $p^* = p_c$. This simplification is equivalent to considering that p_E is negligible with respect to p_c (due to high supersaturation levels); its adoption prevents p^* from being dependent upon the location of the point in the layer because $\boldsymbol{E}_i$ is non-homogeneous. Since p^* is assumed to be constant whatever the macroscopic strain $\boldsymbol{E}$ applied on the system, it can be interpreted as a fluid pressure acting at the interface of the growing crystals. Further, the behavior of the constituents being linear, the superposition principle is used again to decompose the macroscopic loading $(\boldsymbol{\Sigma}_i, p^*)$ exerted on a representative volume element (RVE) of the layer i in the two sub-problems $(\boldsymbol{\Sigma}_i^{(1)} = \boldsymbol{\Sigma}_i + p^*\boldsymbol{I},\ p^* = 0)$ and $(\boldsymbol{\Sigma}_i^{(2)} = -p^*\boldsymbol{I},$

$p^*=0$), denoted $P^{(1)}$ and $P^{(2)}$, respectively. Fig. 9 illustrates this decomposition. The RVE is of course supposed to be statistically representative of the layer and is composed of two sub-domains: Ω designates both C–S–H matrix and non-growing inclusions (CH and porosity) considered as a unique homogeneous constituent and ω represents the growing inclusions (AF crystals). It should be emphasized that the pressure p^* inside the material exerts at the interface of crystals and matrix, although the figure does not reflect this point well.

The local stress and strain tensors are denoted σ_i and ε_i, respectively. The classical volume average over any volume, V, designated by $\langle\cdot\rangle_V$, is defined by:

$$\langle f\rangle_V = \frac{1}{V}\int_V f\,\mathrm{d}V. \tag{26}$$

The problem $P^{(2)}$ as previously defined is trivial; indeed, it is clear that one has:

$$\langle\varepsilon_i^{(2)}\rangle_\Omega = \langle\varepsilon_i^{(2)}\rangle_\omega = \boldsymbol{E}_i^{(2)} = -\frac{p^*}{3k_\Omega}\boldsymbol{I} \tag{27}$$

with k_Ω as the bulk modulus of the domain Ω. The macroscopic strain $\boldsymbol{E}_i^{(1)}$ of the problem $P^{(1)}$ is given by $\boldsymbol{E}_i^{(1)}=\boldsymbol{E}_i-\boldsymbol{E}_i^{(2)}=\boldsymbol{C}_\Omega^{\mathrm{h}^{-1}}:(\boldsymbol{\Sigma}_i+p^*\boldsymbol{I})$, where $\boldsymbol{C}_\Omega^{\mathrm{h}}$ is the (homogenized) stiffness tensor of the layer i, the domain ω being considered as voids. This identity permits, together with the expression of $\boldsymbol{E}_i^{(2)}$, to establish the following relation:

$$\begin{aligned}\boldsymbol{\Sigma}_i &= C_\Omega^{\mathrm{h}}:\left(\boldsymbol{E}_i-\boldsymbol{E}_i^{(2)}\right)-p^*\boldsymbol{I}\\ &= C_\Omega^{h}:\boldsymbol{E}_i-\left(1-\frac{k_\Omega^{\mathrm{h}}}{k_\Omega}\right)p^*\boldsymbol{I}\end{aligned} \tag{28}$$

with $9k_\Omega^{\mathrm{h}}=\boldsymbol{C}_\Omega^{\mathrm{h}}:\boldsymbol{I}:\boldsymbol{I}$. An identification of this formula with Eq. (14) gives the following result, well known in the context of poroelasticity (see e.g. Refs. [34–37]):

$$b_i = 1-\frac{k_\Omega^{\mathrm{h}}}{k_\Omega}. \tag{29}$$

5.1.1. Application

To illustrate the previous theoretical results, a simple numerical application regarding the effects of crystal expansions on the material macroscopic response is provided in terms of maximal percentage of induced stress generated by crystal growth, with respect to the effective crystal pressure p^*. The configuration of the composite sphere model retained for the application corresponds to Figs. 1 and 2, where the anhydrous phase is supposed to be completely hydrated and the outer C–S–H is divided into two layers with different properties (in particular regarding the porosity volume fraction), as explained in Section 3.1; each sphere of the assemblage is then composed of a core and two layers. This construction obeys the macroscopic stress–strain relation (Eq. (13)), with isotropic overall Biot coefficient given by Eq. (23); the Biot coefficient for each sphere layer is expressed by Eq. (29) and the effective pressure exerted by the growing crystals is formulated by Eq. (25) with $p_{\mathrm{E}}=0$. For simplification, both core and external layers are assumed to have a zero Biot coefficient, such that the macroscopic Biot coefficient is:

$$\hat{b}_3 = \frac{b_2(3k_3+4\mu_3)(1-\phi_3)(3k_1+4\mu_2)\phi_2}{9k_1k_2\phi_3(1-\phi_3)+12\mu_2\tilde{k}_{12}\phi_3+(4\mu_3+3k_3(1-\phi_3))(4\mu_2(1-\phi_3)+3\tilde{k}_{12})}. \tag{30}$$

This simplified hypothesis is equivalent to assuming the absence of growing crystals (AF inclusions) in the core and the incorrect fulfillment of the confinement condition in the external layer (which could be explained by its low stiffness due to the relatively important level of capillary porosity), such that the pressure exerted by crystals is negligible. The induced stresses are evaluated by considering that the material undergoes no macroscopic strain, *i.e.* $\boldsymbol{E}=0$, yielding the macroscopic stresses $\boldsymbol{\Sigma}=-\hat{b}_3p^*\boldsymbol{I}$. Once p^* is known locally via the activities of the reactants, the stresses are then directly related to it via $\hat{b}_3$. To illustrate the evolutions of this coefficient with respect to the parameters involved in its expression in a simple way, it is proposed to evaluate the ratio $\hat{b}_3/b_2$ as a function of ratios k_3/k_2, k_1/k_2, μ_3/k_3 and μ_2/k_2, the last two being kept constant and equal to 0.5. Fig. 10 presents the curves $\hat{b}_3/b_2$ versus ϕ_2 for different ratios k_3/k_2 and k_1/k_2 (the values of k_1 indicated in the legend implicitly consider that $k_2=1$) and for several values of ϕ_3; ϕ_1 results obviously from the identity $\phi_1=1-\phi_2-\phi_3$. These values are chosen by considering that the core possesses the greater mechanical properties, followed by the first layer and the second one (subscripts 1, 2 and 3, respectively). As could be expected from Eq. (30), the maximal and minimal values of $\hat{b}_3/b_2$ are obtained for $\phi_2=1$ and $\phi_2=0$, respectively. The influence of k_1/k_2 is all the more important when ϕ_1 is high (or equivalently ϕ_3 is low). The strong variations of $\hat{b}_3/b_2$ with these parameters suggest that they

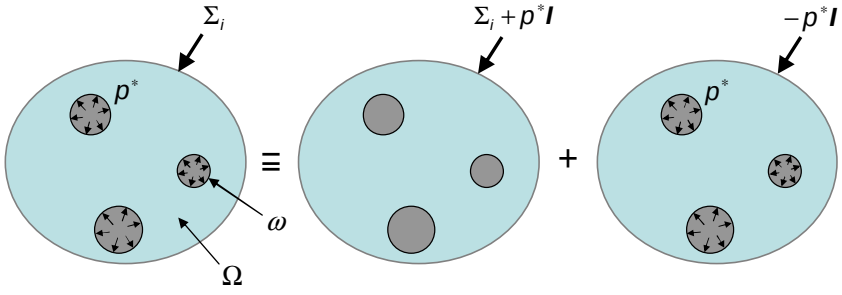

Fig. 9. Decomposition of the macroscopic and internal loading exerting on a RVE of the layer i.

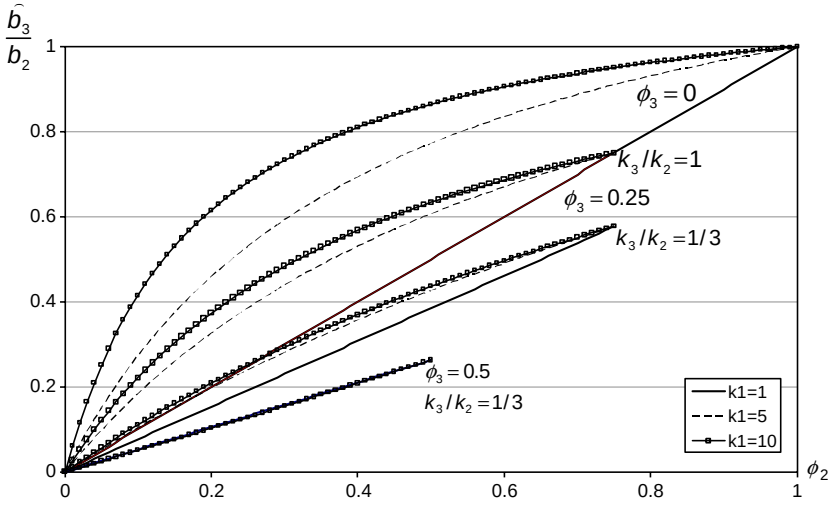

Fig. 10. Evolutions of the ratio $\hat{b}_3/b_2$ defined in Eq. (30) as a function of ϕ_2 for different values of parameters k_1 and k_3 (with $k_2=1$) and porosity ϕ_3.

must be characterized precisely. Finally, it is clear that if all the elastic moduli are lessened by the same factor during a degradation process (decalcification, for example), then $\hat{b}_3/b_2$ does not evolve at constant volume fraction of constituents.

The evaluation of the Biot coefficient b_2 requires the knowledge of mechanical properties for CH inclusions and C–S–H matrix. Making use of the Maxwell approximation method (see e.g. Ref. [16]) for estimating k_Ω^{h} and k_Ω appearing in Eq. (29), b_2 then takes the form:

$$b_2 = 1 - \frac{\left(k_{\mathrm{CSH}} + \frac{4}{3}\mu_{\mathrm{CSH}}\left(\phi_{\mathrm{CH}}\kappa_{\mathrm{CH}} - (\phi_p + \phi_{\mathrm{AF}})\kappa_p\right)\right)\left(1 - \left(\phi_{\mathrm{CH}}\kappa_{\mathrm{CH}} - \phi_p\kappa_p\right)\right)}{\left(1 - \left(\phi_{\mathrm{CH}}\kappa_{\mathrm{CH}} - (\phi_p + \phi_{\mathrm{AF}})\kappa_p\right)\right)\left(k_{\mathrm{CSH}} + \frac{4}{3}\mu_{\mathrm{CSH}}\left(\phi_{\mathrm{CH}}\kappa_{\mathrm{CH}} - \phi_p\kappa_p\right)\right)} \quad (31)$$

with $\kappa_{\mathrm{CH}}=(k_{\mathrm{CH}}-k_{\mathrm{CSH}})/(k_{\mathrm{CH}}+4/3\mu_{\mathrm{CSH}})$ and $\kappa_{\mathrm{p}}=3k_{\mathrm{CSH}}/4\mu_{\mathrm{CSH}}$. To illustrate the evolutions of b_2 as given by the above equation with the volume fraction of AF inclusions ϕ_{AF} in the layer 2, several simulations for different values of CH and porosity volume fractions are performed and gathered in Fig. 11. The following numerical values, drawn from Refs. [9,10], are retained for the computations: $k_{\mathrm{CH}}=38$ GPa, $k_{\mathrm{CSH}}=27$ GPa, and $\mu_{\mathrm{CSH}}=20$ GPa. As expected, the numerical results show that the impact of these latter two quantities is less significant than that of ϕ_{AF}; in particular, the effect of ϕ_{CH} appears to be weak, which is not surprising when considering that its mechanical properties are relatively close to those of the C–S–H matrix.

To conclude this section, the numerical results regarding the evaluation of b_3 as defined by Eq. (30) clearly show the strong dependence on the volume fractions of the different constituents, from the global volume fractions of the coatings forming the composite spheres to the relative ones of the inclusions distributed through them. Concerning this latter aspect, the most influential parameters appear to be the volume fractions of AF and porosity, the one of CH being of less importance due to its mechanical properties being relatively close to those of C–S–H matrix. These results also illustrate the significant impact of the mechanical parameters on the Biot coefficient estimation.

6. Conclusion

This paper addresses the problem of estimating the diffusive and some mechanical properties of cement pastes by making use of both properties and volume fractions of

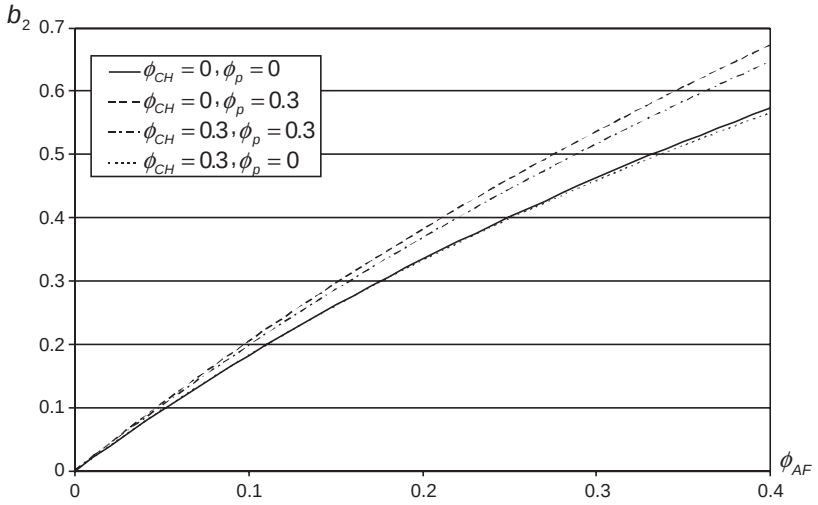

Fig. 11. Evolutions of b_2 as a function of ϕ_{AF} for different volume fractions of CH and porosity, as given by the Maxwell approximation method.

their main hydrated constituents. The description of the material microstructure relies on the adaptation of the multi-coated sphere assemblage model, where the core is constituted of the anhydrous part of the initial cement grain (if it exists) and the first and second layers represent inner and outer C–S–H, respectively (this decomposition is enhanced by dividing this outer layer into two sub-coatings for taking into account the particular behavior of capillary porosity and aluminate inclusions regarding the effective diffusion parameter and expansion phenomena due to sulfate attack, respectively). The other major hydrated products, namely CH and AF, together with the capillary porosity are homogeneously distributed through the C–S–H layers as spherical inclusions. Whereas the macroscopic diffusion coefficient as well as effective Biot coefficient are exactly determined for the composite sphere model, the knowledge of these properties for the sphere constituents (except the core) requires the application of appropriate approximation techniques (the Maxwell and self-consistent methods are used in this study) for taking into account the effects of the spherical inclusions. The developed method is firstly applied to the evaluation of the diffusion coefficient for cement pastes with different water/cement ratios; comparison of the results with available experimental data shows quite good agreement. It is then applied to the estimation of the diffusion coefficient for cement pastes subjected to leaching and carbonation, these two degradation processes being described by using a simplified chemical approach. Further dedicated experiments would be necessary to validate these simulation results. Finally, on the basis of the crystallization pressure concept, the method is extended to the case of the sulfate attack, which induces expansions via the growing of AF inclusions. The method then gives a qualitative description of the major phenomena experimentally observed and is also capable to provide quantitative results when the chemical activities of the reactants present in pore solution are known.

These results suppose that both volume fractions and mechanical properties of the major constituents can be precisely measured, which constitutes an experimental difficulty. In the case of sulfate attack, a subsequent paper will address the whole chemo-transfer-mechanical problem, where the internal crystallization pressure generated by the growing inclusions as defined in this paper will be coupled to a chemo-transfer modeling, for the determination of the concentration in pore solution of the main ionic species. Another aspect of further developments resides in the extension of this approach to the concrete case by inserting aggregate inclusions to the cement paste matrix.

References

[1] A. Lioure, B. Porzio, P. Jaecki, C. Moitrier, I. Tirel, C. Villard, C. Leroy, A. Marvy, D. Iracane, Long-Term Interim Storage of Thermal HLW: Importance, Constraints and Principles for the Management of Long Times in Storage, Int. Conf. GLOBAL 2001, Paris, 2001.

[2] M.C.R. Farage, J. Sercombe, C. Gallé, Rehydration and microstructure of cement paste after heating at temperatures up to 300 °C, Cem. Concr. Res. 33 (2003) 1047–1056.

[3] L.M. Schwartz, E.J. Garboczi, D.P. Bentz, Interfacial transport in porous media: application to dc electrical conductivity of mortars, J. Appl. Phys. 78 (10) (1995) 5898–5908.

[4] E.J. Garboczi, D.P. Bentz, Multiscale analytical/numerical theory of the diffusivity of concrete, Adv. Cem. Based Mat. 8 (1998) 77–88.

[5] Z. Hashin, P.J.M. Monteiro, An inverse method to determine the elastic properties of the interphase between the aggregate and the cement paste, Cem. Concr. Res. 32 (2002) 1291–1300.

[6] I.G. Richardson, The nature of the hydration products in hardened cement pastes, Cem. Concr. Compos. 22 (2000) 97–113.

[7] S. Béjaoui, H. Peycelon, P. Le Bescop, Determination of the effective diffusion coefficients of cement pastes on the basis of a simplified micro/macro homogenization method—application to the modelling of degradation, Euromat 2003, Lausanne, Switzerland, 2003, September.

[8] H.F.W. Taylor, in: Thomas Telford (Ed.), Cement Chemistry, Second edition, London, 1997.

[9] F.H. Heukamp, Chemomechanics of calcium leaching of cement-based materials at different scales: the role of CH dissolution and C–S–H degradation on strength and durability performance of materials and structures, PhD dissertation, MIT, Cambridge, 2002.

[10] C. Constantinides, F.-J. Ulm, The effect of two types of C–S–H on the elasticity of cement-based materials: results from nanoindentation and micromechanical modeling, Cem. Concr. Res. 34 (2004) 67–80.

[11] Z. Hashin, The elastic moduli of heterogeneous materials, J. Appl. Mech. 29 (1962) 143–150.

[12] K. Schulgasser, Concerning the effective transverse conductivity of a two-dimensional two-phase material, Int. J. Heat Mass Transfer 20 (1977) 1273–1280.

[13] G.W. Milton, Concerning bounds on the transport and mechanical properties of multicomponent composite materials, Appl. Phys., A 26 (1981) 125–130.

[14] R.M. Christensen, K.H. Lo, Solutions for effective shear properties in three phase sphere and cylinder models, J. Mech. Phys. Solids 27 (1979) 315–330.

[15] E. Hervé, A. Zaoui, *n*-layered inclusion-based micromechanical modelling, Int. J. Sci. 31 (1) (1993) 1–10.

[16] S. Torquato, Random Heterogeneous Media: Microstructure and Macroscopic Properties, Springer-Verlag, New York, 2001.

[17] G.W. Milton, The Theory of Composites, Cambridge University Press, Cambridge, 2002.

[18] E.J. Garboczi, D.P. Bentz, The effect of statistical fluctuation, finite size error, and digital resolution on the phase percolation and transport properties of the NIST cement hydration model, Cem. Concr. Res. 31 (2001) 1501–1514.

[19] P. Tennis, H.M. Jennings, A model for two types of calcium silicate hydrate in the microstructure of Portland cement pastes, Cem. Concr. Res. 30 (2000) 855–863.

[20] F. Adenot, M. Buil, Modelling of the corrosion of the cement paste by deionized water, Cem. Concr. Res. 22 (1992) 489–496.

[21] P. Faucon, F. Adenot, J.F. Jacquinot, J.C. Petit, R. Cabrillac, M. Jorda, Long-term behaviour of cement pastes used for nuclear waste disposal: review of physico-chemical mechanisms of water degradation, Cem. Concr. Res. 28 (6) (1998) 847–857.

[22] B. Gérard, Contribution des couplages mécanique-chimie-transfert dans la tenue à long terme des ouvrages de stockage de déchets radioactifs, PhD thesis, ENS-Cachan, France, 1996.

[23] B. Bary, A. Sellier, Coupled moisture–carbon dioxide–calcium transfer model for carbonation of concrete, Cem. Concr. Res. 34 (2004) 1859–1872.

[24] J. van der Lee, L. De Windt, V. Lagneau, P. Goblet, Module-oriented modeling of reactive transport with HYTECH, Comput. Geosci. 29 (2003) 265–275.

[25] C. Gallé, H. Peycelon, P. Le Bescop, Effect of an accelerated chemical degradation on water permeability and pore structure of cement-based materials. Submitted for publication to Advances in Cement Research, (2004).

[26] H.F.W. Taylor, C. Famy, K.L. Scrivener, Delayed ettringite formation, Cem. Concr. Res. 31 (2001) 683–693.

[27] J. Skalny, J. Marchand, I. Odler, Sulfate Attack on Concrete, E & FN SPON, London, UK, 2001.
[28] M. Collepardi, A state-of-the-art review on delayed ettringite attack on concrete, Cem. Concr. Compos. 25 (2003) 401–407.
[29] J. Marchand, E. Samson, Y. Maltais, J.J. Beaudoin, Theoretical analysis of the effect of weak sodium sulfate solutions on the durability of concrete, Cem. Concr. Compos. 24 (2002) 317–329.
[30] J. Sercombe, D. Planel, P. Le Bescop, F. Adenot, A. Sellier, B. Capra, J.-M. Torrenti, Calcium Leaching of Cement Paste in Sulfated Water: Relation Between Internal Pressure Kinetics and Crack Initiation. Int. Conf. CONCREEP'6, 2001 (August 20–22). Cambridge, USA.
[31] Xie Ping, J.J. Beaudoin, Mechanism of sulphate expansion: I. Thermodynamic principle of crystallization pressure, Cem. Concr. Res. 22 (1992) 631–640.
[32] XiePing, J.J. Beaudoin, Mechanism of sulphate expansion: II. Validation of thermodynamic theory, Cem. Concr. Res. 22 (1992) 845–854.
[33] G.W. Scherer, Crystallization in pores, Cem. Concr. Res. 29 (1999) 1347–1358.
[34] M.A. Biot, General theory of three-dimensional consolidation, J. Appl. Phys. 12 (2) (1941) 155–164.
[35] M.A. Biot, Theory of elasticity and consolidation for a porous anisotropic solid, J. Appl. Phys. 26 (1955) 182–185.
[36] O. Coussy, Mechanics of Porous Continua, Wiley, New York, 1995.
[37] L. Dormieux, A. Molinari, D. Kondo, Micromechanical approach to the behavior of poroelastic materials, J. Mech. Phys. Solids 50 (10) (2002) 2203–2231.
[38] E. Hervé, Thermal and thermoelastic behaviour of multiply coated inclusion-reinforced composites, Int. J. Solids Struct. 39 (2002) 1041–1058.
[39] V.M. Levin, Thermal expansion coefficients of heterogeneous materials, Mech. Solids 21 (1967) 9–17.